Fermi Surface of $SrFe_2P_2$ Determined by the de Haas–van Alphen Effect

J. G. Analytis,[1,2] C. M. J. Andrew,[3] A. I. Coldea,[3] A. McCollam,[4] J.-H. Chu,[1,2] R. D. McDonald,[5] I. R. Fisher,[1,2] and A. Carrington[3]

[1]*Stanford Institute for Materials and Energy Sciences, SLAC National Accelerator Laboratory, 2575 Sand Hill Road, Menlo Park, California 94025, USA*

[2]*Geballe Laboratory for Advanced Materials and Department of Applied Physics, Stanford University, Stanford, California 94305-4045, USA*

[3]*H. H. Wills Physics Laboratory, University of Bristol, Tyndall Avenue, Bristol, BS8 1TL, United Kingdom*

[4]*Radboud University Nijmegen, High Field Magnet Laboratory, Faculty of Science, 6500 GL Nijmegen, The Netherlands*

[5]*Los Alamos National Laboratory, Los Alamos, New Mexico 87545, USA*

(Received 15 April 2009; published 10 August 2009)

We report measurements of the Fermi surface (FS) of the ternary iron-phosphide $SrFe_2P_2$ using the de Haas–van Alphen effect. The calculated FS of this compound is very similar to $SrFe_2As_2$, the parent compound of the high temperature superconductors. Our data show that the Fermi surface is composed of two electron and two hole sheets in agreement with band-structure calculations. Several of the sheets show strong c-axis warping emphasizing the importance of three dimensionality in the nonmagnetic state of the ternary pnictides. We find that the electron and hole pockets have a different topology, implying that this material does not satisfy a (π, π) nesting condition.

DOI: 10.1103/PhysRevLett.103.076401 PACS numbers: 71.18.+y, 74.25.Jb, 74.70.−b

Many theories of superconductivity and magnetism in iron pnictides have their unusual Fermi surface topology as a central ingredient [1–4]. Both superconductivity and magnetism can be enhanced by geometrical nesting of the hole and electron Fermi surface sheets. Band-structure calculations suggest that 1111 arsenides (RFeAsO$_{1-x}F_x$, $R \in$ La $\rightarrow$ Sm) have stronger ''nesting'' peaks in the noninteracting susceptibility than their 122 arsenide (XFe$_2$As$_2$, $X \in$ Eu, Ba, Sr, Ca) counterparts and the former generally have a higher T_c. The 122 materials are calculated to have stronger warping of their quasi-two-dimensional sheets and experimentally this is reflected in a more isotropic upper critical field H_{c2}.

One argument against a predominant role of Fermi surface nesting is that the phosphide analogues of the 122 arsenide materials (XFe$_2$P$_2$) do not show superconducting or magnetic order despite their calculated Fermi surfaces being very similar to the corresponding arsenides. However, partial substitution of As by P in EuFe$_2$(As$_{1-x}$P$_x$)$_2$ [5] and BaFe$_2$(As$_{1-x}$P$_x$)$_2$ [6] suppresses the antiferromagnetic order and results in superconductivity with T_c up to 26 and 30 K, respectively. The evolution from antiferromagetism to superconductivity and then to paramagnetism in this series provides a strong test of our understanding of the physics of these materials. A particular question is whether this is driven by changes in the Fermi surface topology. Although band-structure calculations can provide a guide, accurate experimental determinations are essential because inaccuracies in the calculated band energies (often of order 0.1 eV [7]) can lead to significant changes in the topology.

Quantum oscillation (QO) studies prove a direct way to probe in detail the bulk, full three-dimensional Fermi surface, and can also resolve the strength of the many-body interactions at the Fermi level. However, so far QO experiments have not been possible on the high T_c superconducting arsenides because of their high H_{c2} and disorder induced by doping. Here we present a de Haas–van Alphen effect determination of the Fermi surface topology and effective masses of $SrFe_2P_2$ which is the end member of the SrFe$_2$(As$_{1-x}$P$_x$)$_2$ series. We find that the hole and electron sheets have quite different topology implying that a geometric nesting condition is not satisfied. This, perhaps, explains the lack of either superconductivity or magnetic order in this compound. The many-body mass renormalization is strongly sheet dependent and much larger than expected from simple electron-phonon coupling.

High quality single crystals of $SrFe_2P_2$ with residual resistivity ratios $\rho(300\ \mathrm{K})/\rho(1.8\ \mathrm{K})$ greater than 50, were grown from a Sn flux. Torque magnetometry was performed using piezoresistive microcantilevers in high fields [8]. Band-structure calculations were performed using an augmented plane wave plus local orbital method as implemented in the WIEN2K code [9]. For these calculation we used the crystallographic parameters $a = 3.825$ Å, $c = 11.612$ Å, and $z_P = 0.3521$ as determined by Mewis [10].

Figure 1(a) shows the raw torque signal for a single field sweep up to 18 T. de Haas–van Alphen oscillations are observed for fields above ~4 T. In Fig. 1(b) we show the fast Fourier transform (FFT) spectrum of the signal (in inverse field) measured at two angles $\theta = 9°$ and $\theta = 49°$, taken relative to the c axis of the crystal and rotating towards the [100] direction. At all angles the spectrum is dominated by a (split) single peak which we label $\alpha_{1,2}$, and in order to make the other smaller amplitude peaks visible

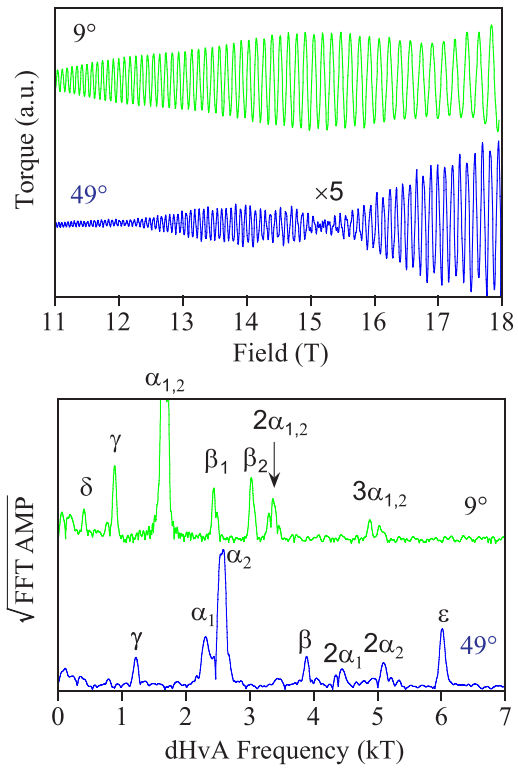

FIG. 1 (color online). dHvA oscillation data in $SrFe_2P_2$ at two different angles. (a) Raw torque signal with smooth polynomial background subtracted; (b) fast Fourier transforms. Note that the y axis is the square root of the FFT amplitude.

we show the square root of the FFT amplitude in the figure. In total seven frequencies are observed, which we denote as α_1, α_2, β_1, β_2, γ, δ, and ϵ, and four others are harmonics of $\alpha_{1,2}$. At higher angle additional splitting of these peaks is observed which likely comes from a small $\sim 1°$ mosaic distribution of the crystal orientation. Note that the FFT peaks below ~ 0.2 kT are noise related. Each of these frequencies are related to a extremal cross sectional area of the Fermi surface (FS) in momentum space A_k via the Onsager relation $F = (\hbar/2\pi e)A_k$.

The calculated Fermi surface for $SrFe_2P_2$ consists of two concentric electron cylinders at Brillouin zone corner, and two hole cylinders centered at the Γ point (see Fig. 2) which is very similar to that calculated for the *nonmagnetic* phase of $SrFe_2As_2$ [11]. All of the sheets are significantly warped.

Rotating away from the c axis we can trace the full three-dimensional topology of the FS by looking at the evolution of the dHvA frequencies as the cyclotron orbits traverse different parts of the FS. Figure 2 (left) shows the angle dependence of each of the observed frequencies with the field being rotated from [001] to [110] on the left and [001] to [100] on the right. There is a high level of correspondence between the observed frequencies and the band structure predictions shown in Fig. 2 (right). The inner electron pocket (band 4) corresponds well to the measured α frequencies, both in absolute cross sectional area (dHvA frequency) and angle dependence (c-axis warping). Similarly, band 3 matches the β orbits. Note the marked differences in angle dependence shown by the β orbits when rotated towards either the [100] or [110] directions. This is well reproduced in the calculations and originates from the highly noncircular shape of this Fermi surface sheet (see Fig. 2). Comparing in detail the absolute frequencies of the α and β with the calculations shows them both to be slightly smaller. A shift of the band energies up by 59 and 49 meV, respectively, for bands 3 and 4 brings them into almost perfect alignment (see Fig. 3).

The ε orbit agrees very well with the maximum frequency from the large hole sheet (band 2), but is observed over only a narrow range of angle (42°–58°). The reason for this is apparent by looking at the slices through the FS shown in Fig. 4, where it can be seen that for this angle there is a large degree of nesting between the warped sections of this band. Indeed, the band-structure calculations show a large increase in the curvature factor

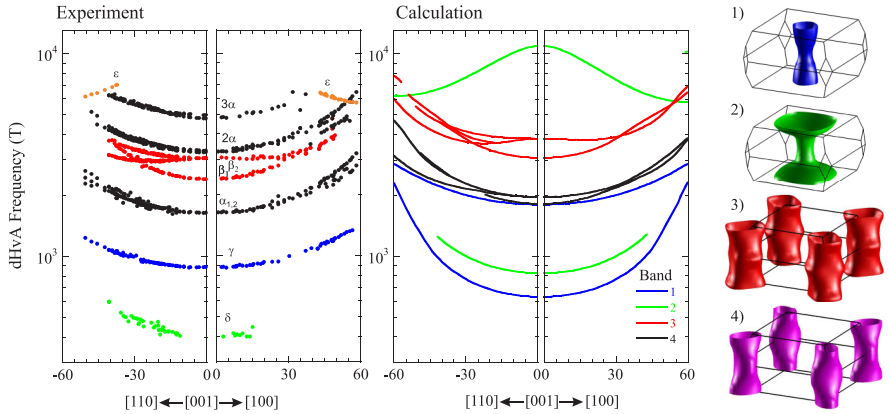

FIG. 2 (color online). Angle dependence of the dHvA frequencies for $SrFe_2P_2$. The left panel of the angle plot shows the experimentally observed frequencies as the magnetic field is rotated from $[110] \rightarrow [001] \rightarrow [100]$. The right panel shows the corresponding predictions of the band-structure calculation. At far right we show the Fermi surfaces associated with each band.

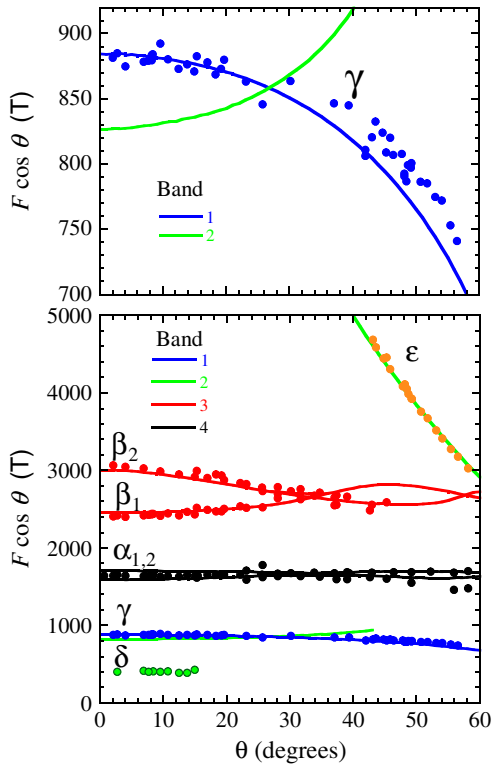

FIG. 3 (color online). Observed dHvA frequencies multiplied by $\cos\theta$ along with band structure predictions for shifted energy bands. The upper panel shows the data for the γ orbit on an expanded scale.

$|\partial^2 A_k/\partial k_{\|}^2|^{-(1/2)}$ (and hence signal amplitude) for these angles.

This leaves frequencies γ and δ to assign. At first glance it appears as though the minima of either band 2 or band 1 could account for these. However, by plotting $F\cos\theta$ versus angle (see Fig. 3) it is apparent that γ cannot be a *minimal* extremal cross section because it decreases as the polar angle increases. Hence, as shown in Fig. 3 the minimum of band 2 has the wrong curvature to explain this orbit. We therefore conclude that this orbit must originate from the maximum of band 1 as this is the only unassigned orbit with the correct local topology. For the frequencies to correspond we need to shift the energies of band 1 down by 110 meV. With this shift the curvature is in good agreement with data (see Fig. 3). Importantly, as shown in Fig. 4 this shift causes the band 1 FS to be a closed three-dimensional ellipsoid. With this assignment the remaining δ orbit must come from the minimal (tubular section) of band 2. Only a small change in the warping of this sheet would be needed to get complete agreement.

Figure 3 shows a comparison of all the observed frequencies with the shift band-structure calculations and Fig. 4 shows the resulting changes in the Fermi surface topology. The shifts can be thought of as a fine tuning of the band-structure calculations. For example, for band 3 the shift corresponds to a decrease in its volume by 0.044 electrons per units cell. A test of the consistency of the shift

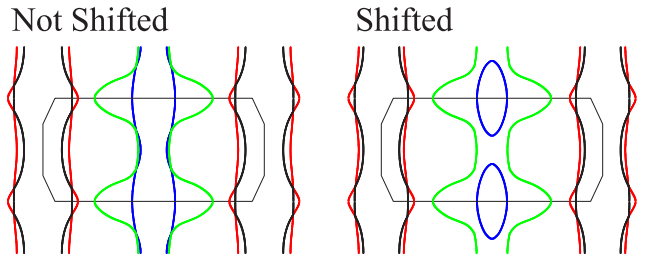

FIG. 4 (color online). Two dimensional sections through the FS in the (110) plane before and after shifting the bands to agree with our dHvA measurements. The Brillouin zone edges are marked.

is to check for charge neutrality. $SrFe_2P_2$ is a compensated metal so the volumes of the electron and hole sheets should be exactly equal. With the shifts bands 1–4 contain -0.026, -0.284, 0.197, and 0.108 holes and electrons, respectively, and so the charge balance remains almost exact. The imbalance of 0.005 extra holes per unit cell is equivalent to $<2\%$ of the total volume of the hole sheets showing the accuracy of our Fermi surface determination.

The effective masses, extracted [8] by fitting the observed temperature dependent amplitude of the dHvA oscillations to the conventional Lifshitz-Kosevich formula [12], are compared in Table I to the corresponding band-structure values. The mass enhancements are strongly sheet dependent and range from $\lambda = m^*/m_b - 1 = 0.3$ for the smallest hole orbit to $\lambda = 1.1$ for the inner electron sheet. These enhancements are similar to those observed in LaFePO [7] and are much larger than expected from electron-phonon coupling alone [13] ($\lambda_{ep} \simeq 0.25$). Table I also shows the orbit specific dHvA mean-free paths. It is interesting to note that, as for LaFePO [7], the electron sheets have the longest mean-free paths and give the strongest dHvA signals. It is not clear to us if there is a fundamental reason for this.

TABLE I. Measured dHvA frequencies, effective masses (m^*), and mean-free paths (ℓ), along with the values from the band-structure calculations. The experimental masses were determined at $\theta = 9°$ except for the ε orbit which is at $\theta = 49°$. The band structure values are all quoted at $\theta = 0°$ ($H \parallel [001]$). The final columns show the ratio of measured effective mass to the band mass at the same angle (at $\theta = 49°$ $m_b = 1.98 m_e$ for 2_{max}).

	Experiment			Calculations			
	F(kT)	$\frac{m^*}{m_e}$	ℓ (nm)	Orbit	F(kT)	$\frac{m_b}{m_e}$	$\frac{m^*}{m_b}$
				1_{min}	0.632	0.97	
γ	0.89	1.49(2)	58	1_{max}	1.804	1.07	1.4
δ	0.41	1.6(1)	21	2_{min}	0.828	1.24	1.3
ϵ	6.02*	3.41(5)*	90	2_{max}	10.95	2.30	1.7
β_1	2.41	1.92(2)	63	3_{min}	3.077	1.25	1.6
β_2	3.06	2.41(3)	70	3_{max}	3.824	1.70	1.6
α_1	1.637	1.13(1)	100	4_{min}	1.823	0.55	2.1
α_2	1.671	1.13(1)	100	4_{max}	1.966	0.60	2.1

The above illustrates that $SrFe_2P_2$ has a FS which is highly dispersive in the c axis and the electron and hole pockets are far from fulfilling a nesting condition. This may explain the observation of an almost isotropic H_{c2} in the analogous hole and electron doped superconducting 122 arsenides [14,15]. In LaFePO, the hole and electron FS sheets are much closer in shape and size [7,16] and this proximity to (π, π) nesting may well be a factor in determining why LaFePO superconducts while $SrFe_2P_2$ does not.

The differences with $SrFe_2As_2$ appear more complicated to answer because the phosphides and arsenides have much in common in their local structure: the As and P ions are isoelectronic, they have a similar atomic radius (100 and 115 pm, respectively), comparable ionization energies and Coulomb interactions [17] and the Pn-Pn distance is large compared with their respective molecular bond lengths (except for $CaFe_2P_2$, which is more analogous to the collapsed tetragonal phase of $CaFe_2As_2$). However, it is important to notice that the 122 arsenides have Pn-Fe-Pn (Pn denotes pnictide) bond angles close to the ideal tetrahedral angle of 109.47°. In the phosphides, however, these bond angles are much larger, and for $SrFe_2P_2$ is 116.34° [18]. The Fe-Pn distance is also smaller by ~0.13 Å in the arsenides, leading to a different bonding overlap. In particular, this results in differences in the calculated pnictogen density of states [19] which Yildirim has argued can dramatically alter the local magnetism of the Fe atoms [20].

The Pn-Fe-Pn bond angle departs from an ideal tetrahedral angle in both LaFePO (119.3°) and $SrFe_2P_2$ (116.34°) in a similar manner and this may be why neither of these compounds exhibits magnetic order. This naturally accounts for the observed suppression of magnetism as $SrFe_2As_2$ is doped with P. However, superconductivity arises at intermediate doping, and this implies that the magnetic order remains important. At some doping, the FS undergoes a reconstruction from that measured in the magnetically ordered state [11], to that measured in this work. We suggest that local interactions and a proximity to nesting work together to enhance T_c. The lower T_c of the 122 compounds as compared to the 1111 compounds is then explained by the absence of nesting [1–4], and the phosphides have a much lower T_c than the arsenides because of the absence of local magnetic interactions [21–24].

In conclusion, we have mapped out the full three-dimensional Fermi surface of $SrFe_2P_2$, the isoelectronic sister compound to the antiferromagnet $SrFe_2As_2$. The Fermi surface is in good overall agreement with the prediction of our band-structure calculations with shifts in the band energies. Unlike LaFePO the Fermi surface of $SrFe_2P_2$ is far from fulfilling a geometric nesting condition, being composed of warped 2D electron cylinders, a strongly warped outer hole cylinder, and one closed hole pocket. The nonmagnetically ordered, nonsuperconducting ground state of $SrFe_2P_2$ is likely related to the combined absence of nesting and local moment interactions, compared to the analogous arsenides.

The authors would like to thank E. A. Yelland for technical assistance. Part of this work has been done with the financial support of EPSRC, Royal Society and EU 6th Framework Contract No. RII3-CT-2004-506239. Work at Stanford was supported by the U.S. DOE, Office of Basic Energy Sciences under Contract No. DE-AC02-76SF00515.

[1] A. V. Chubukov, D. V. Efremov, and I. Eremin, Phys. Rev. B **78**, 134512 (2008).
[2] I. I. Mazin, D. J. Singh, M. D. Johannes, and M. H. Du, Phys. Rev. Lett. **101**, 057003 (2008).
[3] V. Stanev, J. Kang, and Z. Tesanovic, Phys. Rev. B **78**, 184509 (2008).
[4] Y. Ran, F. Wang, H. Zhai, A. Vishwanath, and D.-H. Lee, Phys. Rev. B **79**, 014505 (2009).
[5] Z. Ren *et al.*, Phys. Rev. Lett. **102**, 137002 (2009).
[6] S. Jiang *et al.*, arXiv:0901.3227.
[7] A. I. Coldea *et al.*, Phys. Rev. Lett. **101**, 216402 (2008).
[8] See EPAPS Document No. E-PRLTAO-103-048934 for details about the different samples measured and the effective mass determinations. For more information on EPAPS, see http://www.aip.org/pubservs/epaps.html.
[9] P. Blaha, K. Schwarz, G. K. H. Madsen, D. Kvasnicka, and J. Luitz, *WIEN2K, an Augmented Plane Wave + Local Orbitals Program for Calculating Crystal Properties* (Karlheinz Schwarz, Techn. Universität Wien, Austria, 2001).
[10] A. Mewis, Z. Naturforsch. **35B**, 391 (1980).
[11] S. E. Sebastian *et al.*, J. Phys. Condens. Matter **20**, 422203 (2008).
[12] D. Shoenberg, *Magnetic Oscillations in Metals* (Cambridge University Press, London, 1984).
[13] L. Boeri, O. Dolgovand, and A. Golubov, Physica (Amsterdam) **469C**, 628 (2009).
[14] M. M. Altarawneh *et al.*, Phys. Rev. B **78**, 220505(R) (2008).
[15] H. Q. Yuan *et al.*, Nature (London) **457**, 565 (2009).
[16] H. Sugawara *et al.*, J. Phys. Soc. Jpn. **77**, 113711 (2008).
[17] W. A. Harrison, *Elementary Electronic Structure* (World Scientific Publishing Company, Singapore, 2004), revised ed., ISBN 9812387080.
[18] R. Hoffmann and C. Zheng, J. Phys. Chem. **89**, 4175 (1985).
[19] E. Gustenau, P. Herzig, and A. Neckel, J. Alloys Compd. **262–263**, 516 (1997).
[20] T. Yildirim, Phys. Rev. Lett. **101**, 057010 (2008).
[21] C. Fang, H. Yao, W.-F. Tsai, J. P. Hu, and S. A. Kivelson, Phys. Rev. B **77**, 224509 (2008).
[22] Y. Qi and C. Xu, arXiv:0812.0016.
[23] K. Haule, J. H. Shim, and G. Kotliar, Phys. Rev. Lett. **100**, 226402 (2008).
[24] Q. Si and E. Abrahams, Phys. Rev. Lett. **101**, 076401 (2008).